DOI: 10.1002/chem.201101588

Electroactive Self-Assembled Monolayers of Unique Geometric Structures by Using Rigid Norbornylogous Bridges

Nadim Darwish,[a] Paul K. Eggers,[a] Paulo Da Silva,[a] Yi Zhang,[b] Yujin Tong,[b] Shen Ye,*[b] J. Justin Gooding,*[a] and Michael N. Paddon-Row*[a]

Abstract: Herein, we describe the synthesis of straight (S) and L-shaped (L) norbornylogous bridges (NBs) with an anthraquinone moiety at the distal end as the redox-active head group and two thiol feet at the proximal end, by which the molecules assemble on gold surfaces. The NB molecules were shown to form self-assembled monolayers (SAMs) with a well-behaved surface redox process. The SAMs were characterized by using in situ IR spectroscopy, cyclic voltammetry, scanning tunnelling microscopy and electrochemical impedance spectroscopy. The surface selection rules associated with the IR band intensities allowed the estimation of the position of the anthraquinone moiety with respect to the surface and the tilt of the bridge with respect to the surface normal, both in pure and diluted monolayers. It is shown that the S- and L-NBs hold the plane of the anthraquinone moiety close to the surface normal or the surface tangent, respectively. Neither NB molecule changes its orientation if spaced by diluents on the surface. The difference in the structure of the S- and L-NB SAMs provides a suitable framework for the investigation of factors that govern electron transfer of anthraquinone moieties across self-assembled monolayers with limited structural ambiguity, as compared with the commonly used structurally flexible alkanethiol monolayers.

Keywords: anthraquinones · bridging ligands · electrochemistry · IR spectroscopy · monolayers

Introduction

Quinone derivatives play an important role in biological systems and are attractive for the preparation of electro-active devices.[1,2] In particular, quinone derivatives are important to understand the proton-coupled electron-transfer (ET) reactions that are critical steps in photosynthesis, cellular respiration and mitochondrial ATP synthesis.[3] The most popular quinoid compounds are anthraquinone derivatives, which have a wide variety of uses in such areas as hydrogen peroxide production, oxygen reduction and as a molecular carrier.[4–6] In biological species, quinone derivatives are typically membrane-bound and redox reactions occur at the aqueous–biomembrane interface.[7] Therefore, a detailed knowledge of their surface chemistry and how their interface with the electrolyte affects their ET is critical to the understanding of ET in biological systems. Quinone-terminated self-assembled monolayers (SAMs) have also been highlighted for such applications as electrochemically gated transistors.[8,9] Because the redox potential of quinones can be altered by using the pH of the electrolyte, they can be exploited to obtain a pH-gated transistor.[8]

Despite numerous studies that investigate redox-active SAMs with a wide range of redox-active groups, only a few studies have investigated quinone derivatives as the redox-active terminal group.[2,10–19] Conformationally flexible alkanethiols that mediate between the quinone moieties and the gold surface are often used. The flexible nature of the backbone of an alkanethiol results in ambiguity as to the actual position of the redox reaction centre. This problem is important because the position and the environment around the redox-active group at interfaces can significantly influence the ET reaction. This problem can be overcome by using rigid norbornylogous bridges (NBs) with well-defined organization of the anchoring points to the gold surface and the positioning of the redox centre relative to the surface. The NB molecules can hold the quinone moiety at a well-understood distance and orientation above the surface, defined as the distal end of the diluents in mixed monolayers.

Polynorborane bicyclo[2.2.0]hexane bridges, referred to as norbornylogous bridges, have the properties required to investigate ET processes across SAMs with limited structural ambiguity compared with those previously achieved with flexible alkanethiols.[20,21] NB is a versatile spacer, which is particularly useful for several reasons. Firstly, the bridge is

[a] Dr. N. Darwish, Dr. P. K. Eggers, Dr. P. Da Silva, Prof. Dr. J. J. Gooding, Prof. Dr. M. N. Paddon-Row
School of Chemistry
The University of New South Wales
Sydney, NSW, 2052 (Australia)
Fax: (+612) 93855384
E-mail: justin.gooding@unsw.edu.au
m.paddonrow@unsw.edu.au

[b] Dr. Y. Zhang, Dr. Y. Tong, Prof. S. Ye
Catalysis Research Centre
Hokkaido University
Sapporo 001-0021 (Japan)
Fax: (+81) 11-706-9126
E-mail: ye@cat.hokudai.ac.jp

Supporting information for this article is available on the WWW under http://dx.doi.org/10.1002/chem.201101588.

structurally rigid, which means that the terminal redox moiety is held in a fixed, well-defined orientation. Secondly, the nature of the bridge allows systematic variation of the length and configuration, which allows a study of the dependence on distance and the effect of bridge configuration on the dynamics of the ET. Finally, the nature of the NBs allows a wide range of redox-active moieties to be attached to the termini.[22–28]

In previous studies using an ellipsometry technique, SAMs formed from tetrathiolated NBs (Scheme 1a) were shown to tilt by an angle of about 30 to 34° to the surface

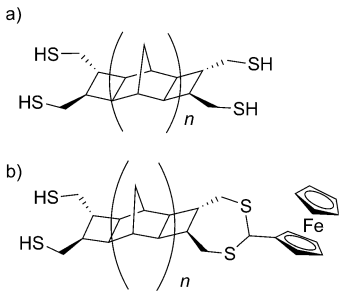

Scheme 1. a) Tetrathiolated and b) ferrocene-terminated NBs.

normal.[29] It was suggested that both thiol groups bond to the gold surface and that the NB molecules are more stable on the gold surface compared with other commonly used alkanethiols.[29] Eggers et al. studied a series of NB molecules with a ferrocene (Fc) moiety fused to one end of the NB bridge (Scheme 1b).[30] In situ IR spectroscopy was used to show that the NB molecules change their tilt angle during the redox reaction (Fc to Fc^+) in SAMs formed from ferrocene-terminated NBs only.[30] The change in tilt angle was ascribed to the space requirement needed for the Fc^+ to bind to the ClO_4^- counterions. However, in mixed SAMs composed of NB molecules diluted with shorter alkanethiols, the NB molecules did not change their orientation during the redox reaction. The fixed orientation was explained by the ability of the NB molecules to lift the ferrocene moiety above the surface defined by the distal end of the diluents. In such a position, the ferricinium cations are not sterically congested and, therefore, ion pairing with ClO_4^- does not necessitate a change in the tilt angle of the bridge.[30]

This paper has two aims. The first is to describe the synthesis of straight and L-shaped NB compounds (S- and L-NB, respectively) that are terminated at one end with anthraquinone moieties and with two vicinal (CH_2SH) groups in a *trans* relationship at the proximal end. The second is to investigate the surface and electrochemical properties of the SAMs formed from these molecules on gold surfaces by using in situ IR spectroscopy, scanning tunnelling microscopy and electrochemical impedance spectroscopy.

Four criteria were taken into consideration when designing the NB compounds described in this paper:

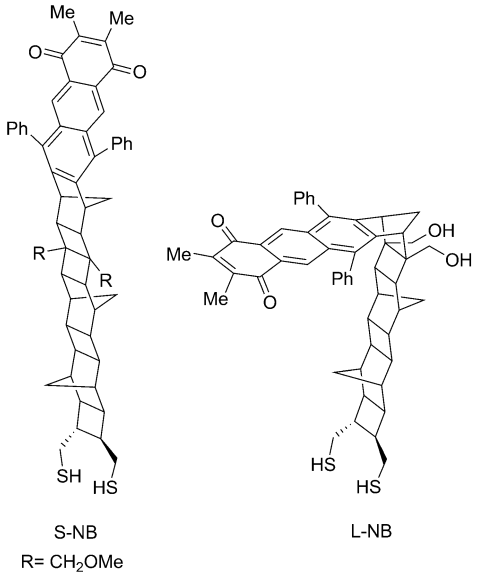

1) The molecules are totally rigid, which allows precise knowledge of the position of the redox-active moiety.
2) The difference in the structures of the S- and L-NBs allows two different orientations of the anthraquinone moiety with respect to the gold surface or the surface of diluents in mixed monolayers. This difference allows investigation of both the effect of the orientation of the redox active group on the electron transfer process and also how the diluent in a mixed SAM affects electron transfer.
3) The molecules are long enough to be able to position the anthraquinone redox-active group above the surface of the diluents in a mixed monolayer. A short bridge necessitates the use of shorter diluents, which is known to form less-ordered SAMs.[31] To address this issue, the S- and L-NB molecules were synthesised to be longer than 14 Å.
4) The molecules possess a *trans* CH_2SH stereochemistry at the proximal end, at which the molecules bond to the gold surface. These "feet" lend more rigid anchoring points to the gold surface.

Figure 1 presents the geometry-optimized structures of the S- and L-NB molecules performed by using density functional theory at the B3LYP/6-31G(d) level of theory.[32] The distance between the thiol groups and the carbonyl groups for L- and S-NB is 14.2 and 19.9 Å, respectively. The synthetic procedure leads to the formation of a racemic modification that is not resolved and is directly used in the preparation of the SAMs because both enantiomers should bond in an identical fashion to the gold surface.[29]

Results and Discussion

The synthesis of S- and L-NBs followed standard procedures.[33,34] Key steps are depicted in Scheme 2 and detailed

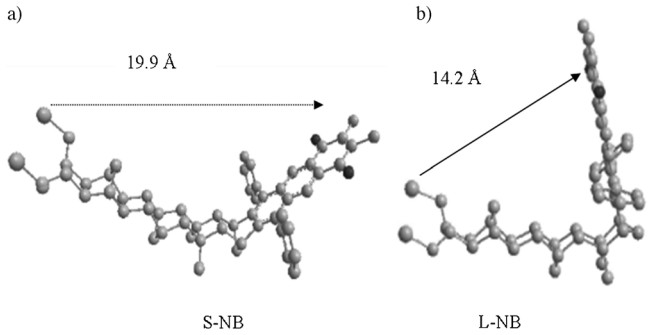

Figure 1. B3LYP/6-31G(d)-optimized structure of a) S-NB and b) L-NB; distances shown are between the thiol groups and the carbonyl groups. The OCH_3 groups in the backbone of S-NB and the OH groups in the backbone of the L-NB were omitted for clarity.

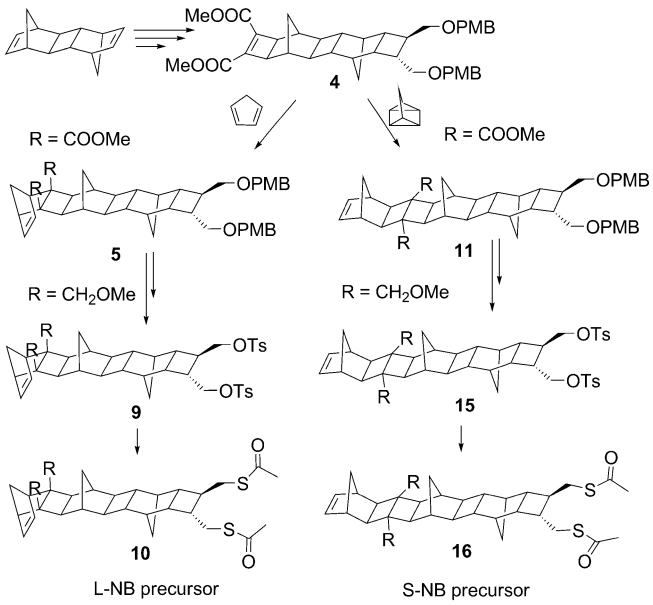

Scheme 2. Synthesis of the L- and S-NB precursors. Full schemes and experimental procedures are presented in the Supporting Information.

schemes and experimental procedures are presented in the Supporting Information. The norbornadiene dimer underwent a ruthenium-catalyzed thermal [2+2] cycloaddition of dimethyl acetylenedicarboxylate (DMAD),[35] followed by reduction of the esters to give hydroxyl groups protected with *para*-methoxybenzyl groups (PMB). The NB was then extended from the other side by a second cycloaddition of DMAD to give key compound **4**. The L-NB precursor was achieved by treating **4** with cyclopentadiene to give **5**. The *exo*-isomer selectivity of the cyclopentadiene addition was confirmed by the X-ray structure of **9** (Figure 2). The *exo*-isomer selectivity agrees with those reported previously for similar reactions.[34,36,37] The synthesis of the S-NB precursor was achieved by a similar procedure to the one used for L-NB. However, instead of treating **4** with cyclopentadiene to give the L-NB precursor, compound **4** was treated with quadricyclane to give the S-NB precursor. The final targets

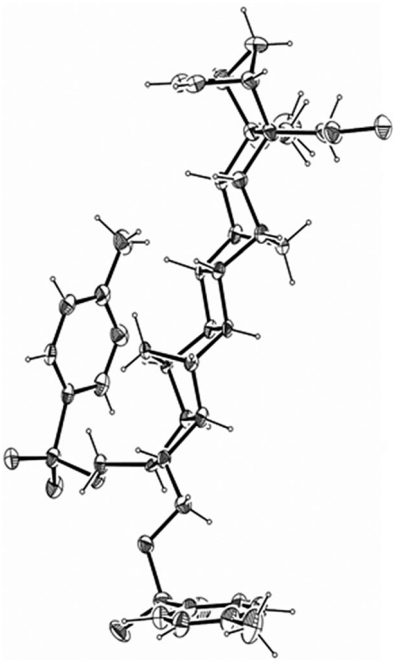

Figure 2. ORTEP diagram of the X-ray crystal structure of the L-NB precursor (**9**), showing the *exo*-addition of cyclopentadiene and the *trans* relationship of the two CH_2OTs groups. Ellipsoids were drawn at the 50% probability level.

were then achieved by reacting precursors **10** and **16** with 6-7-dimethyl-1,3-diphenyl-naphtho[2,3-*c*]furan-5,8-dione (INF)[38] by using a Diels–Alder reaction followed by dehydration[36] to produce the anthraquinone moiety (Scheme 3). The reaction of INF with the NB was characterized by X-

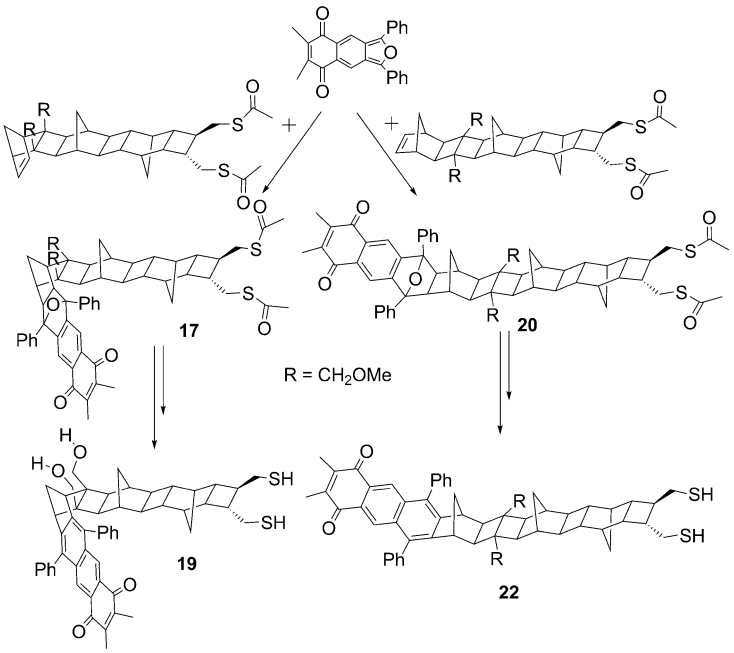

Scheme 3. The anthraquinone moiety was achieved by treating the S- and L-NB precursors with INF followed by dehydration.

ray crystallography (see the Supporting Information). Both the Diels–Alder and the dehydration reaction required harsher conditions for the L-NB compound than for the S-NB compound. This difference in behaviour is probably due to the steric hindrance present in the L-NB, which makes the Diels–Alder and the dehydration reaction comparatively more difficult. In contrast to the dehydration of S-NB using trifluoroacetic acid (TFA) at 40°C, the dehydration reaction for L-NB was achieved by using *para*-toluenesulfonic acid (PTSA) in dry benzene under reflux and inert atmospheric conditions. These conditions were also sufficient to cleave the methoxy groups at the cyclobutane ring to form hydroxyl groups at that position instead.

Characterisation of pure monolayers: The anthraquinone moiety undergoes a $2e^-$, $2H^+$ redox reaction in aqueous electrolytes (Figure 3a, inset).[39] Cyclic voltammetry (CV) performed on the pure S- and L-NB SAMs (Figure 3a) showed oxidation and reduction waves that are ascribed to the oxidation and reduction of the anthraquinone moiety. The area under the Faradaic peaks is similar for both the S- and L-NB SAMs, which indicates that the molecules in each SAM have nearly the same surface coverage of $(5.20\pm0.5)\times10^{13}$ molecules cm^{-2}; this translates to around 1.92 nm^2 $molecule^{-1}$. At first, this similarity in surface coverage obtained from CV may be surprising, but considering the dimensions of the molecules (in-plane and out-of-plane, Figure S2 in the Supporting Information) and the conformation of the two CH_2SH groups on the surface (ascertained by using in situ IR spectroscopy; see below), the area needed for each S-NB is 1.60 nm^2 $molecule^{-1}$, which is comparable to the value of 1.76 nm^2 $molecule^{-1}$ calculated for L-NB (see Figure S2 in the Supporting Information). When a voltage of −750 mV is applied to the electrode, the anthraquinone redox moiety is reduced to the anthrahydroquinone. The IR spectra at −750 mV (Figure 3b) are subtracted from an IR spectrum at 0 mV, at which the anthraquinone moiety is in its oxidized form. This leads to differential spectra in which the downward bands (decrease in the IR absorption) are related to the consumption of the anthraquinone species and the upward bands (increase in the IR absorption) are related to the formation of anthrahydroquinone species. According to surface selection rules on highly reflective metal surfaces,[40] bonds that are perfectly parallel to the surface should be invisible in the IR spectrum. Thus, it is only possible to observe IR bands for bonds that have a vertical component relative to the surface.[41–43] Figure 3b presents the IR spectra of SAMs formed from either the S- or the L-NB molecules (i.e., in the absence of diluents). The downward bands at 1662 cm^{-1} are assigned to C=O stretching in the anthraquinone moiety. Bands at similar frequencies were previously reported for the C=O stretch in benzoquinone (BQ) species in solution (1672 cm^{-1}),[44] C=O in the oxidized form of thiolated hydroquinone SAMs, that is, H_2QSH (1647 cm^{-1}),[18] H_2QC_1SH (1650 cm^{-1})[45] and 2-(11-mercaptoundecyl) hydroquinone (1660 cm^{-1})[14] SAMs

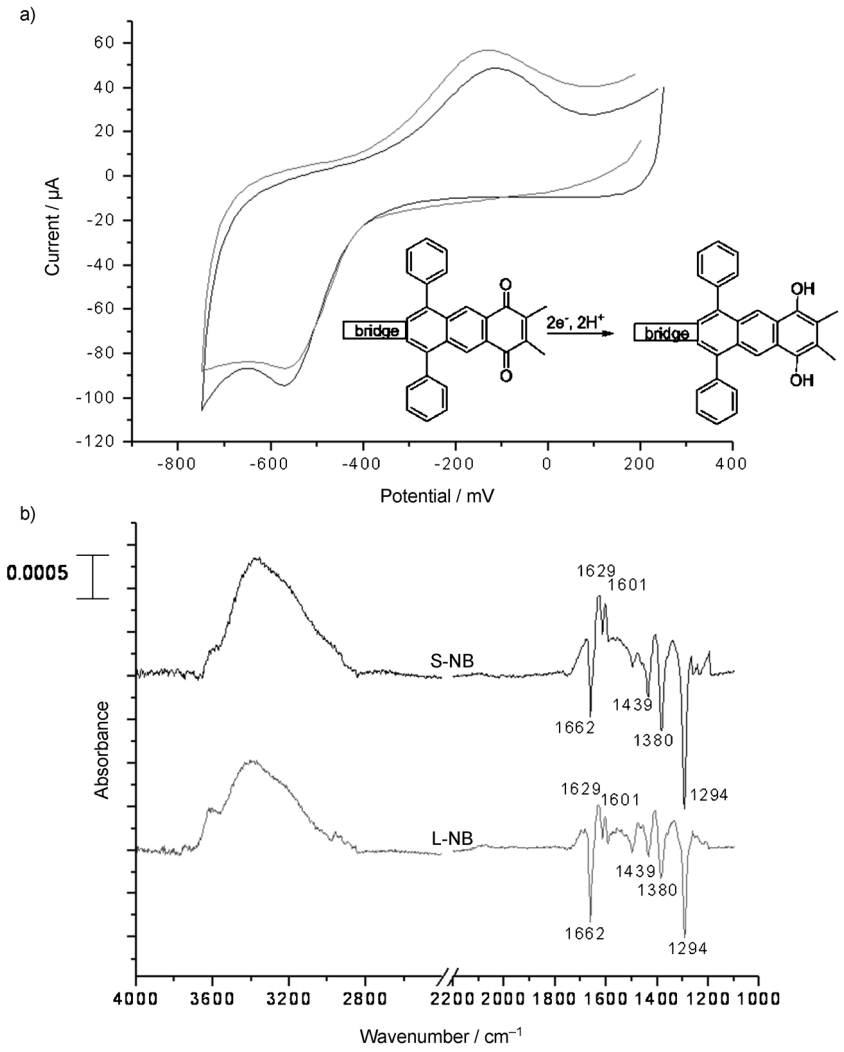

Figure 3. a) Cyclic voltammograms of pure S- (——) and L-NB (——) SAMs at 250 mV s^{-1}, pH 7.4. b) In situ IR spectra of pure S- (——) and L-NB (——) SAMs at −750 mV subtracted from an IR spectrum recorded at 0 mV.

on gold surfaces. The upward bands at 1601 and 1629 cm^{-1} are both assigned to the aromatic C=C skeletal stretch of the benzene ring in the anthrahydroquinone form (species appearing). The wavenumbers are close to those reported for an aromatic ring C=C stretching of 1626[46] and 1580, 1598 cm^{-1}[47] for anthrahydroquinone derivatives in solution and to the 1580 cm^{-1} upward band corresponding to the C=C of SAMs formed from 2-(11-mercaptoundecyl) hydroquinone on a gold surface by using in situ IR spectroscopy.[14] The IR spectra for both S- and L-NB SAMs at different surface potentials are presented in Figure S6 (Supporting Information).

The downward bands at 1294, 1380 and 1439 cm^{-1} are all assigned to the C–C stretch of the quinone ring in the anthraquinone form. These bands are close to those reported for the ring C–C stretching of 1,4-naphthoquinone and 9,10-anthraquinone in solution (1295, 1328, 1370, 1452 cm^{-1})[47,48] and to the 1333 and 1293 cm^{-1} ring C–C stretching of anthraquinone-2-carboxylic acid on gold surfaces.[49] The large upward band between 2870 and 3600 cm^{-1} is assigned to the O–H stretching of water. Because an upward band represents an increase in the IR absorption compared with that at the reference potential (0 mV vs. Ag/AgCl), the increase in the intensity of the O–H stretching at −750 mV can be attributed to an increase in the quantity of water at the interface as the terminal groups switch from the anthraquinone species (at 0 mV) to the more hydrophilic anthrahydroquinone species (at −750 mV). The assignment of the IR bands for both S- and L-NB SAMs are summarized in Table 1. The

Table 1. Assignment of the upward and downward IR bands observed for the S- and L-NB monolayers.

Assignment	Wavenumber [cm^{-1}]
C=O	1662
C=C stretching (upward)	1601, 1629
C–C stretching (downward)	1294, 1380, 1439
O–H bending	2870–3600

in situ IR spectra for the pure S- and L-NB SAMs showed the same number of IR bands at the same wavenumbers (Figure 3b and Table 1). However, the relative band intensities in each SAM, are different. The intensity ratio of the bands assigned for the C–C stretching of the quinone ring (1439, 1380, 1294 cm^{-1}) to the carbonyl band (1662 cm^{-1}) is larger for the S-NB SAM than for the L-NB SAM. The difference in behaviour suggests that the C–C bonds of the quinone ring in the S-NB molecule are more normal to the surface compared with that of the L-NB.

The observation of bands representing anthraquinone and anthrahydroquinone moieties indicates that the quinone moiety in both compounds possesses a vertical component with respect to the surface. As mentioned in the introduction, the S- and L-NB molecules have the same backbone and the same points of adhesion to the gold surface (2× CH_2SH). Therefore, it is expected that the conformation of the two CH_2SH groups on the surface will be similar for both molecules. To determine the conformation of the CH_2SH groups, an IR band that corresponds to a functional group that maintains the same vertical component and, therefore, has a similar intensity in both SAMs should be identified. The carbonyl groups on the anthraquinone in the S- and L-NB SAMs will have a similar vertical component to the surface regardless of any possible conformation of the two CH_2SH groups. Therefore, the intensity of the IR band of the carbonyl groups (1662 cm^{-1}) can be used as an internal standard to which the intensities of other bands are compared. Unlike the similar orientation of the carbonyl groups in each SAM, the orientation of the C–C and the C=C bonds in the quinone/hydroquinone ring will be different for each SAM; this orientation depends on the conformation of the two CH_2SH points of attachment to the gold surface. Table 2 presents the IR band intensities of the (C=C and

Table 2. IR band intensities normalized to the carbonyl band at 1662 cm^{-1}.

Wavenumber [cm^{-1}]	L-NB	S-NB
1662 (carbonyl)	1.0	1.0
1629 (upward) C=C aromatic anthrahydroquinone	0.24	0.52
1601 (upward) C=C aromatic anthrahydroquinone	0.26	0.48
1439 (downward) C–C anthraquinone	0.25	0.51
1380 (downward) C–C anthraquinone	0.63	1.24
1294 (downward) C–C anthraquinone	1.1	1.97

C–C) of the anthraquinone moiety normalized to the band intensity of the internal standard (C=O). The normalized band intensities (Table 2), of the C–C and the C=C bonds of the quinone/hydroquinone ring in both the oxidized and the reduced form of the S-NB SAM are larger by an average factor of around 1.9 than that of the L-NB SAM. The larger factor in the S-NB SAM is attributed to the greater vertical component of the C–C (quinone) and the C=C (hydroquinone) bonds in S-NB compared with L-NB. This indicates that the L-NB molecules place the anthraquinone moiety in a position at which it is more parallel to the gold surface. Based on this, it is possible to deduce the conformation of the CH_2SH groups on the gold surface that best describe the IR data. Figure 4a,b presents a proposed conformation of the CH_2SH groups in the case of the L-NB and Figure 4c,d shows the same conformation of the CH_2SH groups for the S-NB. In both the S- and L-NB molecules, the two CH_2SH groups are pointing in opposite directions and are both bonded to the gold surface. This CH_2SH conformation places the carbonyl groups for both S- and L-NB at the same angle with respect to the gold surface. Conversely, the quinone ring of the L-NB molecule (circled in Figure 4a) is close to parallel with respect to the surface. However, the quinone ring in the S-NB molecule (circled in Figure 4d) is situated closer to the surface normal. Other schematic drawings that represent the orientation of the quinone terminal group are presented in Figure S3 in the Supporting Information. The assembly of each NB molecule on the surface can be sketched as analogous to a runner at the starting gun.

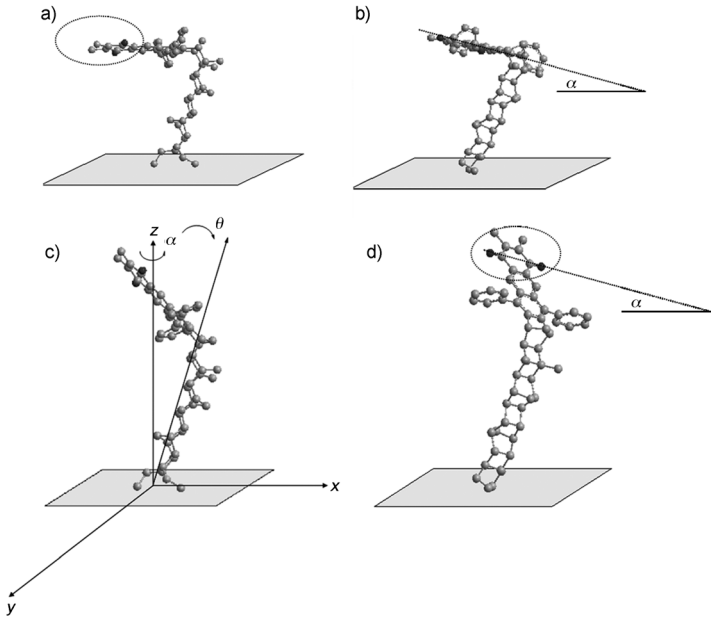

Figure 4. The proposed orientation of a,b) L-NB and c,d) S-NB (two different views). Angle θ is attributed to the NB backbone tilt in the xz plane. Angle α is attributed to the NB backbone tilt in the yz plane. The angle of the carbonyl groups with respect to the gold surface (α) is similar for both the S- and L-NB. The quinone ring (circled in a) and d)) in L-NB has a smaller vertical component with respect to the surface compared with that circled for the S-NB. According to these 3D models, α is $\approx$25° and θ is $\approx$30°.

The knees of the runner (one lower and one higher) resemble the CH_2 groups in a *trans* relationship and the feet resemble the sulfur atoms that are attached to the gold surface (Figure 5). We propose a two-step mechanism for the assembly of the *trans* CH_2SH feet on the gold surface. First, one of the sulfur atoms binds to the gold surface. Second, the other CH_2SH strand rotates around the carbon atom of the CH_2SH group until it allows the other sulfur atom to bind to the gold surface.

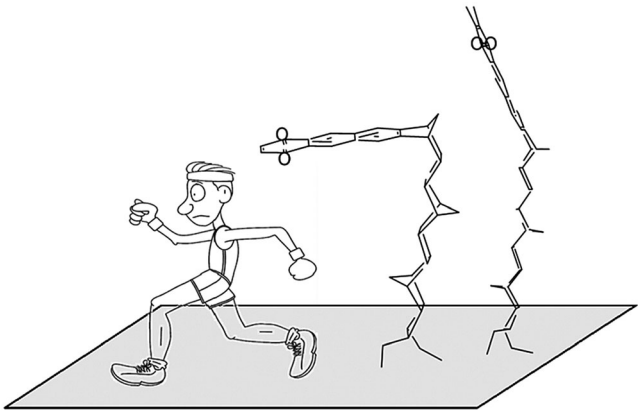

Figure 5. A schematic drawing of a runner at the starting gun alongside the structures of S- and L-NB attached to a gold surface. The runner's knees resemble the carbon atoms of the CH_2SH and his feet resemble the sulfur atoms.

Characterisation of diluted monolayers: Figure 6a presents cyclic voltammograms of a pure SAM formed from L-NB molecules and a diluted SAM formed from a mixture of L-

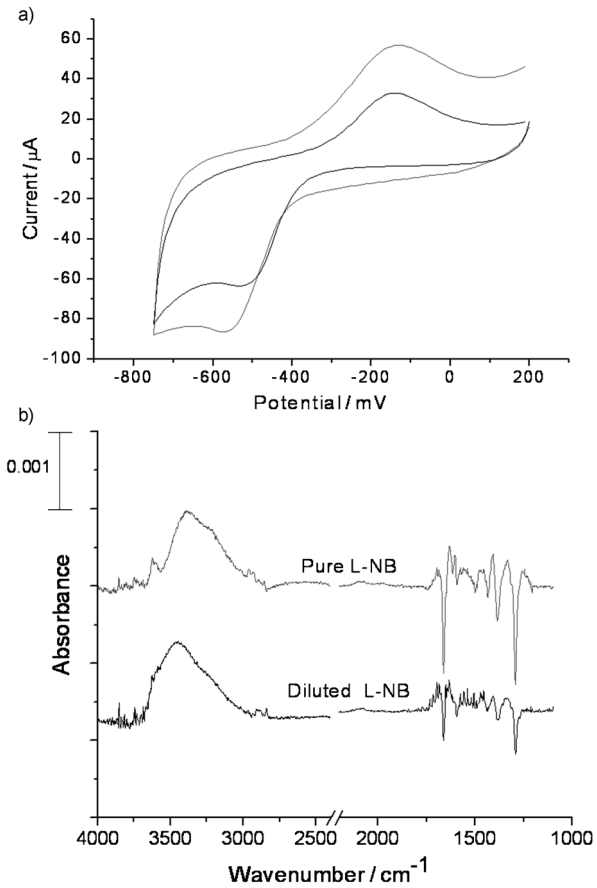

Figure 6. a) Cyclic voltammograms of pure L-NB SAM (——) compared with that of a diluted L-NB/6-mercaptohexan-1-ol SAM (——); scan rate: 250 mV s^{-1}. b) In situ IR spectra of the pure L-NB SAM (——) compared with that of the diluted L-NB/6-mercaptohexan-1-ol SAM (——) at −750 mV.

NBs and 6-mercaptohexan-1-ol (1:4 molar ratio) in solution. From the area under the Faradaic peak, the calculated surface coverage for the NBs in the pure SAM was around 5.20×10^{13} molecules cm^{-2}, whereas that for the diluted monolayer was around 2.60×10^{13} molecules cm^{-2}. The intensities of the IR bands (Figure 6b) in the diluted SAM are weaker than those of the pure SAM, as expected with fewer L-NB molecules present on the surface. The IR band intensities in the diluted SAM preserve the same relative ratio they had in the pure L-NB SAM. In particular, the intensity ratio of the band at 1662 cm^{-1} (C=O stretching) to the intensity of the band at 1294 cm^{-1} (C−C stretching) is 1.05, which is close to the relative ratio of the intensities of these two bands in the pure SAM (1.1). This suggests that the L-NB molecules do not change their orientation on the surface when they are diluted. The composition of the mixed SAM was further diluted to have only a quarter of the NB mole-

cules on the surface; again, the IR bands intensities were scaled proportionally and the IR band intensities diminished to approximately one quarter of the intensity of the bands in the pure SAM. Also, the relative band intensities again preserved the ratio they had in the pure SAM.

The same behaviour was observed for a SAM formed from S-NB molecules diluted with 9-mercaptononan-1-ol (Figure 7a). The surface coverage of the NB molecules calculated from the area under the Faradaic peak for the pure and diluted SAMs (5.20×10^{13} and 3.23×10^{13} molecules cm^{-2}, respectively). As in the case of the diluted L-NB SAM, the band intensities in the diluted S-NB SAM preserved the relative ratio observed in the pure S-NB SAM (Figure 7b). The ratio of the intensity of the band at 1662 cm^{-1} (C=O stretching) to the intensity of the band at 1294 cm^{-1} (C–C stretching) is 1.88, which is close to the relative ratio of these two bands in the pure SAM (1.97). Because the relative intensities of the IR bands are similar for both pure and diluted SAMs, this strongly suggests that the orientation of NB molecules are determined by the conformation of the two CH_2SH groups on the gold surface, and this conformation will be similar whether the NB molecules are spaced by diluents or present as the only component. Therefore, the in-

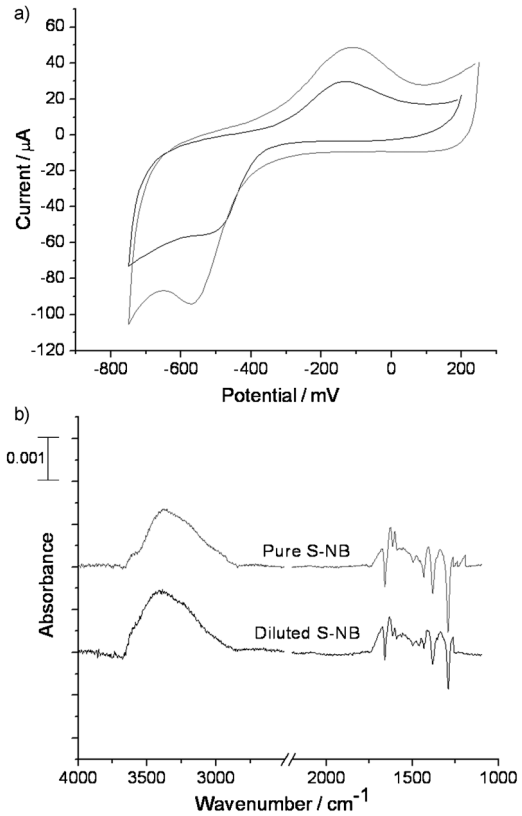

Figure 7. a) Cyclic voltammograms of a pure S-NB SAM (——) compared with that of a diluted S-NB/9-mercaptononan-1-ol SAM (——); scan rate: 250 mV s^{-1}. b) In situ IR spectra of the pure S-NB SAM (——) compared with that of the diluted S-NB/9-mercaptononan-1-ol SAM (——) at −750 mV.

plane tilt (xz plane) and out-of-plane tilt (yz) of the NB molecules shown for the pure SAMs in Figure 4 is retained for NB molecules in the diluted monolayers. This tilt angle is close to the tilt angle suggested for SAMs formed only from alkanethiols.[50,51] Therefore, in mixed NB–alkanethiol SAMs the L-NB molecule will place the anthraquinone moieties very close to parallel to the distal surface of the diluents, whereas the S-NB molecules will place the anthraquinone moieties close to the normal of the distal surface of the diluents.

STM studies and electrochemical impedance spectroscopy of pure SAMs: STM images (Figure 8) reveal that SAMs formed from S- and L-NBs have different structures. In the case of L-NB SAMs (Figure 8b and c), a highly-ordered network-like structure is observed. However, in the case of S-NB SAMs, no network-like structure is observed (Figure 8d and e).

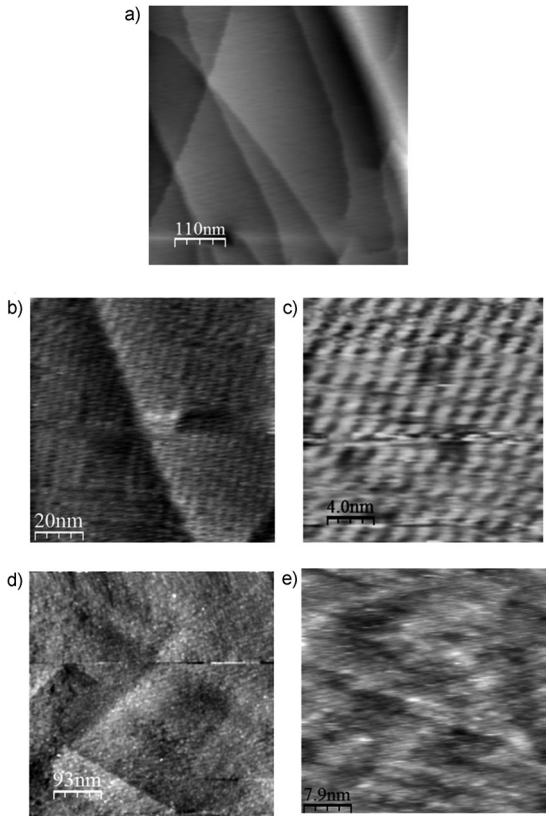

Figure 8. STM images of a) an unmodified (bare) Au (111) single gold crystal surface (570×570 nm, scale bar 110 nm), b) a pure L-NB SAM (100×100 nm, scale bar 20 nm), c) a pure L-NB SAM (20×20 nm, scale bar 4.0 nm), d) a pure S-NB SAM (465×465 nm, scale bar 93 nm), e) a pure S-NB SAM (40×40 nm, scale bar 7.9 nm).

These images agree with the structure of the SAMs suggested by the in situ IR spectroscopy. In the case of the S-NB SAM, the anthraquinone head groups, which are oriented close to the surface normal, are spaced out due to the space required by the backbone of the NBs. However, we

speculate that the nearly parallel orientation of the anthraquinone moieties in the L-NB SAM allows interaction between the anthraquinone head groups on the surface despite the space required for the backbone of the bridges. Therefore, the ordered arrays of L-NB bridges observed may be a consequence of interactions between the anthraquinones. A magnified STM image of the L-NB SAM (5×5 nm, 25 nm^2) appears to have 11 bright spots (Figure S5 in the Supporting Information). Each spot correlates to an individual molecule and, therefore, the area per molecule is 2.3 nm^2. As mentioned above, the area per L-NB molecule calculated by using CV is around 1.92 nm^2 molecule^{-1}, which is reasonably close to the value obtained from the STM images.

The difference in the structure of S- and L-NB SAMs, observed in the STM images, suggests that S-NB SAMs have more space between the anthraquinone moieties than the L-NB SAMs. This hypothesis was explored by using electrochemical impedance spectroscopy (EIS), which averages information over the entire surface area. EIS gives quantitative information on the dielectric properties of the SAMs and, therefore, the accessibility of the underlying gold surface to ions in solution. The measurements were obtained over a frequency range of 100 KHz to 1 Hz and at a dc potential that does not overlap with the Faradaic process (0 V vs. Ag/AgCl). This technique is exceedingly sensitive to any defects in the SAM. The resulting impedance data can be represented as phase angle versus frequency plots, referred to as Bode plots (Figure 9). The phase angle reflects the relative magnitude of the capacitive impedance and the solution resistance. Ideally, the Bode phase plot of a Helmholtz capacitor should give a phase angle of 90° at low frequencies. Deviation of the phase angle from 90° (at low frequencies) would suggest an electrical current leakage through the dielectric layer of the Helmholtz capacitor.[52–54] At higher frequencies, the total impedance is dominated by the solution resistance and the phase angle decreases towards zero. In this study, the Bode phase plot (Figure 9) demonstrates that the L-NB SAM behaves as a close-to-ideal capacitive SAM with a phase angle of about 87°, which indicates an insulating monolayer; Wang et al. suggest that phase angles of 80 to 88° confirm the presence of a highly insulating dielectric material on the electrode surface.[54] Conversely, the phase angle at low frequency for the S-NB SAM was about 77°, which indicates that it is less insulating than the L-NB SAM. A more quantitative information about the structures of the monolayers was obtained by fitting the impedance data to the circuit presented in Figure 10, inset. The resistance of the L-NB SAM ((8.10 ± 0.90) MΩ cm^2) was found to be about an order of magnitude greater than the resistance of the S-NB SAM ((1.10 ± 0.11) MΩ cm^2). This difference in the resistance values for the two SAMs is ascribed to more solvent penetration in the S-NB SAM than in the L-NB SAM. The difference in the dielectric properties can also be inferred from the capacitance values of each SAM. The capacitance of the L-NB SAM is (4.55 ± 0.01) μF cm^{-2}, whereas that of the S-NB SAM is (9.84 ± 0.08) μF cm^{-2}. The capacitance of a monolayer is given by $C=\varepsilon_r\varepsilon_0 A/d$, in which C is the capacitance, ε_r is the dielectric constant of the SAM, ε_0 is the permittivity of free space, A is the surface area and d is the thickness of the monolayer. Therefore, for the systems presented herein there are two factors that are important with regards to the magnitude of the measured capacitance: the dielectric constant of the SAM, which is directly proportional to the capacitance, and the thickness of the film. The higher capacitance of the S-NB SAM can be ascribed to a higher dielectric constant of the S-NB SAM due to solvent penetration through the backbone of the NB molecules. Despite being a thicker film, the solvent penetration in the S-NB SAM increases the dielectric constant of the SAM. The L-NB SAM has a lower capacitance due to a greater ability to block the penetration of the solvent owing to the anthraquinone moieties being held close to parallel to the surface.

The difference in the dielectric properties supports the hypothesis that the anthraquinones form a close packed layer

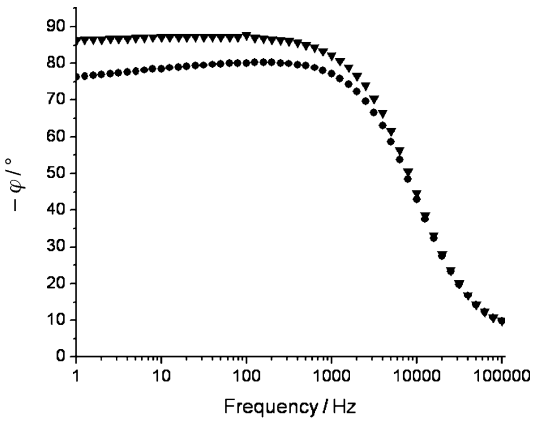

Figure 9. Bode phase plots of S- (●) and L-NB (▼) SAMs. The impedance spectra were obtained at 0 V vs. Ag/AgCl and an ac amplitude of 10 mV at pH 7.4.

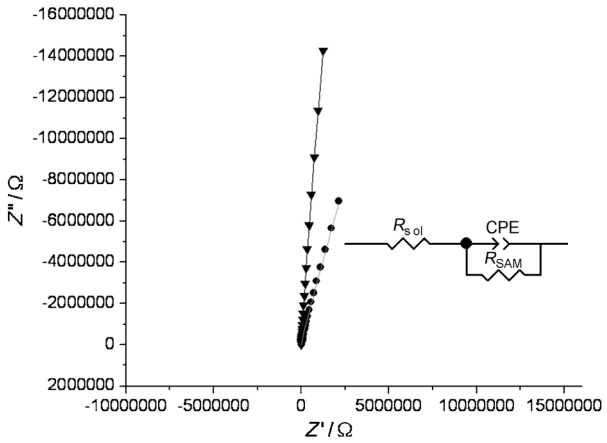

Figure 10. Nyquist plots of the impedance of SAMs formed from L-NB (▼) and S-NB (●); the symbols represent experimental data and the lines are the best fits. Inset: The equivalent circuit used to fit the impedance data. The fitting parameters are presented in Table S1 in the Supporting Information.

in the L-NB SAM, whereas the anthraquinones in the S-NB SAM are not closely associating. The EIS agrees with this hypothesis because the lower penetration of solvent in the L-NB SAM is consistent with the anthraquinone rings forming a shelter over the hydrophobic backbone of the bridge and, therefore, preventing the electrolyte from penetrating through to the electrode surface. Conversely, the anthraquinone moiety in the S-NB SAM does not form a complete shelter and, therefore, cannot completely block the electrolyte from penetrating through the backbone of the NB molecules. The difference in the dielectric properties of both SAMs further indicates that the L-NB molecules hold the anthraquinone groups parallel to the gold surface, whereas the S-NB molecules place the anthraquinone groups close to the surface normal.

Conclusion

The synthesis of straight and L-shaped NB compounds with an anthraquinone redox-active head group and two thiol groups is described herein. These compounds were shown to form self-assembled monolayers on gold surfaces. In situ IR spectroscopy, STM imaging and the dielectric properties of the SAMs demonstrated that this class of NB molecules can precisely locate the redox moiety in a well-defined orientation with respect to the electrode surface and with respect to the surface of diluents in a mixed monolayer. The anthraquinone rings of SAMs formed from L-NBs were shown to be located close to parallel to the surface, whereas those from SAMs prepared from S-NBs were found to be close to the surface normal. These systems are currently being exploited to study the influence of the environment surrounding the anthraquinone moiety on the redox reaction by forming SAMs in which the environment around the anthraquinone moiety is altered by using diluents of different length and different distal groups.

Experimental Section

In situ IR spectroscopy: 6-Mercaptohexan-1-ol and 9-mercaptononan-1-ol were purchased from Sigma–Aldrich (>98%). The detailed schemes and experimental procedures for the synthesis of S- and L-NBs are given in the Supporting Information. SAMs were formed on gold films (thickness ≈50 nm) that were chemically deposited on the reflecting surface of a hemicylindrical Si prism. The procedure of chemically depositing gold is described elsewhere.[55] Before surface modification with SAMs, the gold surfaces were electrochemically cleaned by scanning the potential between 0.0 and +1.5 V (vs. Ag/AgCl) for 10 cycles in 0.5 M H_2SO_4 to remove possible organic additives adsorbed on the surface during the Au chemical deposition. SAMs formed from pure NB were formed by incubating the surfaces in a solution of NB (1 mM) in dichloromethane (CH_2Cl_2) for 18 h. Mixed SAMs were prepared by incubating the surfaces in a solution of NB and alkanethiol diluent (molar ratio 1:4; total concentration 1 mM) in CH_2Cl_2.[56] The surfaces were incubated in the mixed solution for 20 min, after which they were removed and placed in a solution of alkanethiol (1 mM) in CH_2Cl_2 for 18 h. The in situ IR spectroscopy measurements were carried out by using a BioRad FTS-60A/896 spectrometer equipped with a MCT detector. The IR spectra were recorded in dynamic mode with a spectral resolution of 4 cm^{-1}. Each IR spectrum was recorded during a fixed potential with a waiting time of 100 s. Details of the in situ IR spectroscopy measurements are described elsewhere.[57,58] All IR spectra were subtracted from a spectrum recorded at 0 V (vs. Ag/AgCl) in the same solution in which the anthraquinone was in its oxidized form. All electrochemical experiments were carried out by using an Ivium CompactStat potentiostat (Netherlands) at RT. A three-compartment electrochemical cell was used for electrochemical characterization. The reference electrode was a saturated KCl Ag/AgCl electrode and all potentials are referred to the reference. The counter electrode was a platinum gauze. The electrolyte solution used was phosphate buffer (PBS; 0.1 M, pH 7.4) with a controlled ionic strength of 0.6 M NaCl using NaH_2PO_4, Na_2HPO_4 and NaCl (Wako Pure Chemicals, Japan). The electrolyte solution was deaerated with Ar (99.99%, Hokkaido Air Water, Japan) for at least 15 min before each measurement.

Scanning tunneling microscopy: STM images were acquired by using a Picoscan system (Molecular Imaging Corp., USA) under ambient conditions. SAMs were formed by incubating Au (111) surfaces in a 1 mM solution of the NB compounds prepared in a solution of CH_2Cl_2. The STM tip was prepared by mechanically cutting a Pt/Ir wire. All images were acquired in a constant-current mode. The typical imaging conditions were bias voltages of 0.35 V and a tunnelling current of 25 pA. Images were manipulated with WxSM software (Nanotec, Spain) and the contrast was enhanced by applying a low-pass filter.

Electrochemical impedance spectroscopy: The electrochemical impedance spectroscopy experiments were recorded by using a Solartron 1287 electrochemical interface with a Solartron Impedance/Gain-Phase Analyser. The AC amplitude was 10 mV. Data analysis was carried out by using the program Z View by Scribner Associates. The measurements were performed in a three-electrode cell containing an Au (111) working electrode by forming a meniscus with the electrolyte, a platinum foil counter electrode and a saturated KCl Ag/AgCl reference electrode.

X-ray structure determination: CCDC-826618 (compound **S1** in the Supporting Information) and CCDC-826619 (**9**) contain the supplementary crystallographic data for this paper. These data can be obtained free of charge from The Cambridge Crystallographic Data Centre via www.ccdc.cam.ac.uk/data_request/cif.

Acknowledgements

N.D. acknowledges ARCNN for a travel fellowship to Hokkaido University, Japan. The Australian Research Council under the Discovery Projects Funding Scheme (DP0556397) is acknowledged. Dr. Mohan Bhadbhade from the Analytical Center, UNSW, is acknowledged for the X-ray structures presented in this paper. This work was partially supported by a Grant-in-Aid for Exploratory Research (21655074) and a Grant-in-Aid for Scientific Research on Innovative Areas "Coordination Program" (22108501) from MEXT, Japan.

[1] M. Gómez, F. J. González, I. González, *J. Electroanal. Chem.* **2005**, *578*, 193.
[2] A. D. Abhayawardhana, T. C. Sutherland, *J. Phys. Chem. C* **2009**, *113*, 4915.
[3] B. L. Trumpower, *J. Biol. Chem.* **1990**, *265*, 11409.
[4] S. M. Golabi, J. B. Raoof, *J. Electroanal. Chem.* **1996**, *416*, 75.
[5] A. Sarapuu, K. Vaik, D. J. Schiffrin, K. Tammeveski, *J. Electroanal. Chem.* **2003**, *541*, 23.
[6] K. L. Wong, G. Pawin, K.-Y. Kwon, X. Lin, T. Jiao, U. Solanki, R. H. J. Fawcett, L. Bartels, S. Stolbov, T. S. Rahman, *Science* **2007**, *315*, 1391.
[7] M. Matsson, D. Tolstoy, R. Aasa, L. Hederstedt, *Biochemistry* **2000**, *39*, 8617.
[8] P. Petrangolini, A. Alessandrini, L. Berti, P. Facci, *J. Am. Chem. Soc.* **2010**, *132*, 7445.

[9] X. Li, B. Xu, X. Xiao, X. Yang, L. Zang, N. J. Tao, *Faraday Discuss.* **2006**, *131*, 111.
[10] A. T. Hubbard, *Chem. Rev.* **1988**, *88*, 633.
[11] S. A. Trammell, D. A. Lowy, D. S. Seferos, M. Moore, G. C. Bazan, N. Lebedev, *J. Electroanal. Chem.* **2007**, *606*, 33.
[12] S. A. Trammell, M. Moore, T. L. Schull, N. Lebedev, *J. Electroanal. Chem.* **2009**, *628*, 125.
[13] Y. Sato, M. Fujita, F. Mizutani, K. Uosaki, *J. Electroanal. Chem.* **1996**, *409*, 145.
[14] S. Ye, A. Yashiro, Y. Sato, K. Uosaki, *J. Chem. Soc. Faraday Trans.* **1996**, *92*, 3813.
[15] S. A. Trammell, M. Moore, D. Lowy, N. Lebedev, *J. Am. Chem. Soc.* **2008**, *130*, 5579.
[16] W. Zhang, S. M. Rosendahl, I. J. Burgess, *J. Phys. Chem. C* **2010**, *114*, 2738.
[17] A. G. Larsen, K. V. Gothelf, *Langmuir* **2005**, *21*, 1015.
[18] T. Sasaki, I. T. Bae, D. A. Scherson, B. G. Bravo, M. P. Soriaga, *Langmuir* **1990**, *6*, 1234.
[19] J. J. Hickman, D. Ofer, P. E. Laibinis, G. M. Whitesides, M. S. Wrighton, *Science* **1991**, *252*, 688.
[20] A. J. Black, T. T. Wooster, W. E. Geiger, M. N. Paddon-Row, *J. Am. Chem. Soc.* **1993**, *115*, 7924.
[21] T. T. Wooster, P. R. Gamm, W. E. Geiger, A. M. Oliver, A. J. Black, D. C. Craig, M. N. Paddon-Row, *Langmuir* **1996**, *12*, 6616.
[22] M. N. Paddon-Row, *Acc. Chem. Res.* **1982**, *15*, 245.
[23] M. N. Paddon-Row, *Acc. Chem. Res.* **1994**, *27*, 18.
[24] V. Balaji, L. Ng, K. D. Jordan, M. N. Paddon-Row, H. K. Patney, *J. Am. Chem. Soc.* **1987**, *109*, 6957.
[25] A. D. Joran, B. A. Leland, G. G. Geller, J. J. Hopfield, P. B. Dervan, *J. Am. Chem. Soc.* **1984**, *106*, 6090.
[26] S. I. Khan, A. M. Oliver, M. N. Paddon-Row, Y. Rubin, *J. Am. Chem. Soc.* **1993**, *115*, 4919.
[27] K. A. Jolliffe, T. D. M. Bell, K. P. Ghiggino, S. J. Langford, M. N. Paddon-Row, *Angew. Chem.* **1998**, *110*, 959; *Angew. Chem. Int. Ed.* **1998**, *37*, 915.
[28] K. A. Jolliffe, S. J. Langford, A. M. Oliver, M. J. Shephard, M. N. Paddon-Row, *Chem. Eur. J.* **1999**, *5*, 2518.
[29] W. R. Yang, M. W. Jones, X. Li, P. K. Eggers, N. Tao, J. J. Gooding, M. N. Paddon-Row, *J. Phys. Chem. C* **2008**, *112*, 9072.
[30] P. K. Eggers, P. Da Silva, N. A. Darwish, Y. Zhang, Y. Tong, S. Ye, M. N. Paddon-Row, J. J. Gooding, *Langmuir* **2010**, *26*, 15665.
[31] J. J. Gooding, F. Mearns, W. Yang, J. Liu, *Electroanalysis* **2003**, *15*, 81.
[32] W. Koch, M. C. Holthausen, *A Chemist's Guide to Density Functional Theory*, 2nd ed., Wiley-VCH, Weinheim, **2001**.
[33] H. Oevering, M. N. Paddonrow, M. Heppener, A. M. Oliver, E. Cotsaris, J. W. Verhoeven, N. S. Hush, *J. Am. Chem. Soc.* **1987**, *109*, 3258.
[34] R. N. Warrener, I. G. Pitt, D. N. Butler, *Chem. Soc. Chem. Commun.* **1983**, 1340.
[35] T. Mitsudo, K. Kokuryo, T. Shinsugi, Y. Nakagawa, Y. Watanabe, Y. Takegami, *J. Org. Chem.* **1979**, *44*, 4492.
[36] N. J. Head, A. M. Oliver, K. Look, N. R. Lokan, G. A. Jones, M. N. Paddon-Row, *Angew. Chem. Int. Ed.* **1999**, *38*, 3219.
[37] K. Kumar, R. J. Tepper, Y. Zeng, M. B. Zimmt, *J. Org. Chem.* **1995**, *60*, 4051.
[38] B. L. Serpaud, Y. Lepage, *Bull. Soc. Chim. Fr.* **1977**, 539.
[39] S. A. Trammell, N. Lebedev, *J. Electroanal. Chem.* **2009**, *632*, 127.
[40] R. Greenler, *J. Chem. Phys.* **1966**, *44*, 310.
[41] L. Pranger, A. Goldstein, R. Tannenbaum, *Langmuir* **2005**, *21*, 5396.
[42] K. V. G. K. Murty, M. Venkataramanan, T. Pradeep, *Langmuir* **1998**, *14*, 5446.
[43] M. Moskovits, *J. Chem. Phys.* **1982**, *77*, 4408.
[44] B. R. Clark, D. H. Evans, *J. Electroanal. Chem.* **1976**, *69*, 181.
[45] I. T. Bae, M. Sandifer, Y. W. Lee, D. A. Tryk, C. N. Sukenik, D. A. Scherson, *Anal. Chem.* **1995**, *67*, 4508.
[46] M. Umadevi, V. Ramakrishnan, *Spectrochim. Acta Part A: Mol. Spectrosc.* **2003**, *59*, 393.
[47] S. N. S. Singh, R. S. Singh, *Spectrochim. Acta Part A* **1968**, *24*, 1591.
[48] A. Latef, J. C. Bernede, S. Benhida, *Thin Solid Films* **1991**, *195*, 289.
[49] S. W. Han, S. W. Joo, T. H. Ha, Y. Kim, K. Kim, *J. Phys. Chem. B* **2000**, *104*, 11987.
[50] A. Ulman, J. E. Eilers, N. Tillman, *Langmuir* **1989**, *5*, 1147.
[51] K. Sinniah, J. Cheng, S. Terrettaz, J. E. Reutt-Robey, C. J. Miller, *J. Phys. Chem.* **1995**, *99*, 14500.
[52] E. Boubour, R. B. Lennox, *Langmuir* **2000**, *16*, 7464.
[53] E. Boubour, R. B. Lennox, *J. Phys. Chem. B* **2000**, *104*, 9004.
[54] W. Wang, S. Zhang, P. Chinwangso, R. C. Advincula, T. R. Lee, *J. Phys. Chem. C* **2009**, *113*, 3717.
[55] H. Miyake, S. Ye, M. Osawa, *Electrochem. Commun.* **2002**, *4*, 973.
[56] P. K. Eggers, H. M. Zareie, M. N. Paddon-Row, J. J. Gooding, *Langmuir* **2009**, *25*, 11090.
[57] S. Ye, Y. Sato, K. Uosaki, *Langmuir* **1997**, *13*, 3157.
[58] S. Ye, W. Zhou, M. Abe, T. Nishida, L. Cui, K. Uosaki, M. Osawa, Y. Sasaki, *J. Am. Chem. Soc.* **2004**, *126*, 7434.

Received: May 24, 2011
Published online: November 23, 2011

